Research Article

Aerodynamic Modeling and Performance Study of an INVELOX System Containing Multiple Wind Turbines Using a Semi-Analytical Approach

Saeed Karimian Aliabadi [a*], Saber Rezaey [b]

[a] *Faculty of Mechanical Engineering, Tarbiat Modares univesity, Tehran, Iran.*
[b] *M.Sc. in Mechanical Engineeing, Tarbiat Modares university, Tehran, Iran.*

P A P E R   I N F O

A B S T R A C T

The INVELOX system is an innovative approach that offers improved energy absorption efficiency from wind flow and reduced costs by utilizing smaller wind turbines. This research focuses on investigating the steady-state performance of one, two, or three wind turbines arranged within the venturi section of the system. A comprehensive modeling approach using an improved Blade Element Momentum (BEM) theory is proposed and implemented as a MATLAB code. The code incorporates Prandtl's tip and hub loss factors, as well as turbulent wake corrections. The accuracy of the code is validated against experimental and numerical data. The results demonstrate that in a three-rotor tandem configuration in the INVELOX system, the power extracted from the second and third turbines is 0.54 and 0.24 times the power of the first turbine, respectively. Furthermore, for a two-turbine arrangement in the venturi section, the total power extracted from the system is 53.9% higher than that of a single turbine layout. In the case of a three-turbine configuration, the total power increases up to 1.78 times compared to a single turbine. The proposed model is suitable for geometric optimization and parameter studies. The system's performance is evaluated in terms of tip speed ratio, and the effects of different correction models are analyzed, including the local changes in forces and moments.

1. INTRODUCTION

Among all renewable energy systems, wind energy systems require much more consideration in terms of installation, periodic services, and maintenance. Therefore, it is necessary to design a wind turbine intelligently to ensure higher efficiency and lower production cost. Many different types of wind energy systems have been invented so far and much effort has been made to increase the capacity of wind turbines. One of the innovative systems for this task is the INVELOX that enjoys many features and resolve the problems associated with traditional wind systems. The most significant advantage is the use of smaller rotor blades. The design of today's conventional blades is costly and complicated, both in aerodynamics and structure. However, turbine blades using the INVELOX system become more affordable and can be maintained more easily due to smaller size and better accessibility. The first study of ducted wind turbines was conducted by Rainbird and Lily in 1956 (Lilley & Rainbird, 1956). They explored the performance of ducted wind turbines. The results demonstrated that if a suitable design was used for the nozzle-diffuser duct, the output power would be at least 65% greater than the value obtained for the case of no-duct wind turbines. In 2012, another concept of ducted wind turbine called INVELOX was introduced by Allaei

and Andreopoulos (Allaei & Andreopoulos, 2014; Allaei, Tarnowski, & Andreopoulos, 2015) in SheerWind Company. In the initial version of the INVELOX system, the turbine chamber was situated at ground level, and the design aimed to achieve optimal compatibility between the blade and the chamber through its unique configuration. This approach was intended to pave the way for the commercialization of ducted wind turbines by reducing costs associated with installation, maintenance, and production. Figure 1 illustrates the overall layout of the INVELOX wind turbine, as introduced and presented by Allaei and Andreopoulos (Allaei & Andreopoulos, 2014; Allaei, Tarnowski, & Andreopoulos, 2015).

Figure 1. General outline of the INVELOX wind turbine system

* Corresponding Author's Email: Karimian@modares.ac.ir (S. Karimian)
URL: https://www.jree.ir/article_191260.html

Allaei et al. (Allaei & Andreopoulos, 2013) continued their innovative activities by examining and analyzing the use of three turbines in the INVELOX system based on the experiment. By examining the performance of the system with two and three turbines, they found that the system efficiency for two and three turbines increased by 52% and 72%, respectively, compared to that for one turbine. Esfahanian et al. (Fereidoonnezhad, Tahani, & Esfahanian, 2017) studied the performance of ducted turbines using the surface vorticity method. One of the advantages of this method is its time efficiency compared to conventional numerical methods. It relies only on the lift and drag coefficients as input parameters, making it applicable to various types of wind turbines, including ducted wind turbines. Kumar et al. (Kumar, Subathra, & Cota, 2015) designed a small-scale INVELOX system and tested its performance at low speeds using a subsonic wind tunnel. The result showed that the INVELOX system was more efficient than conventional turbines and had the ability to produce power at low wind speeds with appropriate efficiency. Billah and Qasim (Billah & Qasim, 2019) developed a Simulink MATLAB framework for a 3D INVELOX system using fluid continuity principles. They determined the speed ratio between the venturi section and other sections based on the system's geometry. Their results demonstrated that the proposed model accurately calculated the velocity ratio with high efficiency.

Shirazi et al. (Golozar et al., 2021) designed a 3D controllable aerodynamic roof as the input part of the INVELOX system. Using numerical simulations, they concluded that the use of this controllable roof could increase the system efficiency by about 12 percent. Gohar et al. (Gohar et al., 2019) presented a new 3D design for the INVELOX system and analyzed the system using a numerical method. It was revealed that the new design would speed up the wind in the venturi and increase output power. Akour and Bataineh (Akour & Bataineh, 2019) studied and analyzed the effective parameters in the INVELOX system using numerical 3D simulations. They presented an optimal design for the system. It was demonstrated that the highest velocity in the venturi section could be achieved when the body of the INVELOX system would be oriented along 45 or 135 deg. relative to the wind direction. By reducing the diameter of the venturi section of the INVELOX system, Bhatt et al. (Solanki, Kayasth, & Bhatt, 2017) examined the performance and output power of the system based on the 3D computational model. They found that if the existing diameter of venturi section varied from 6ft to 4ft, upstream velocity at the second and third turbines would increase 9.44 m/s to 14.3 m/s and 3.15 m/s to 8.06 m/s, respectively.

Patel and Desmukh (SnehalNarendrabhai & Desmukh, 2018) worked on an INVELOX system and analyzed it by numerical 3D simulations. They deduced that by utilizing the INVELOX, the same 3-bladed built-in turbine could produce 6 to 8 times more energy than the bare turbine. Anbarsooz et al. (Anbarsooz, Hesam, & Moetakef-Imani, 2017) investigated the geometric parameters and the effect on the aerodynamic performance of the INVELOX numerically. Their results showed that the area of the inlet section and the diameter of the venturi section had great effect on the venturi section velocity. Further numerical studies on the effect of geometric parameters of the INVELOX system, such as length and diameter, on the performance were conducted by other researchers (Hosseini & Ganji, 2020; Nardecchia et al., 2020; Wibowo et al., 2018).

Wind turbine blades are responsible for extracting wind energy. The rotor blades are composed of airfoils whose chord and pitch angle distribution are important parameters in the formation of useful local forces. One of the practical methods for achieving optimal chord and pitch angle distribution is the BEM theory. BEM theory or blade element momentum theory is an analytical and practical method for calculating aerodynamic forces generated in horizontal wind turbine rotor blade sections. The BEM can be consequently used to calculate the performance and power of the turbine. The basis of the BEM theory was proposed by Glauert (Glauert, 1926). Hsiao et al. (Hsiao, Bai, & Chong, 2013) studied 3 different types of small-scale horizontal wind turbines with a diameter of 0.72 m experimentally and numerically. They initially proposed the optimum twist and chord distribution. The three rotor layouts selected were an un-tapered and un-twisted blade, un-tapered one with optimum twist distribution, and a tapered blade (optimum chord length distribution) with optimum twist distribution. In this work, a series of wind tunnel tests were scheduled to measure the power coefficient for the three mentioned turbines. The comparison of these layouts was extensively reported.

Tang et al. (Tang et al., 2015) proposed a direct method for design and evaluation of small-size turbine blades. Using a suitable aerodynamic model, they determined the chord and pitch angle distribution by considering the effect of the Reynolds number, tip, and hub loss factor, as well as drag coefficient. BEM theory can be used to analyze and evaluate the turbines that use marine and tidal currents. Masters et al. (Masters et al., 2011) presented a powerful numerical method for this purpose in their work and developed the model embedding the Prandtl's tip and hub loss factor. Rajan et al. (Rajan & Ponta, 2019) provided a new empirical relation to improve and extend BEM theory. The model presented by them is based on numerical analysis applied to the actuator disk model. Tahani et al. (Tahani et al., 2017) designed a 1 MW horizontal axis wind turbine using linear chord and pitch angle distribution to achieve nearly maximum power coefficient. Their results showed that region of 60 to 64 percent the chord and 30 to 37 percent the blade length is the proper area to apply the linear chord and pitch angle distribution.

In addition to the CFD method, which is widely used in the analysis of fluid flow (Rezaey, 2020), many studies have evaluated wind turbines based on theories such as the BEM theory. Vaz et al. (Vaz, Pinho, & Mesquita, 2011) proposed a mathematical model based on BEM theory considering the effect of the turbulent wake on the rotor plane for a horizontal wind turbine. The results demonstrated the good agreement between the new framework and the previous models. Supreeth et al. (Supreeth et al., 2021) investigated the effect of geometry on the wake rotational speed, drag coefficient, and Prandtl's tip loss factor as well as the performance of a 2-kW horizontal axis wind turbine. Their results revealed the interference between the mentioned parameters and the geometry. Aerodynamic performance of the blade and the power coefficient in the optimal design were reportedly reduced by about 25 percent due to mentioned losses. Nabil et al. (Nabil, Khairat Dawood, & Mansour, 2018) adopted an approach to the selection of airfoil and blade design utilized in small horizontal wind turbines with low cut-in speed and no gear box. Krishna et al. (Krishna, Bhargava, & Donepudi, 2018) used the BEM theory to evaluate a horizontal axis wind turbine equipped with a twist-angle change control system. Many other researchers

(Bavanish & Thyagarajan, 2013; Karimian Aliabadi & Rasekh, 2019; Karimian Aliabadi & Rezaey, 2022; Liu, Wang, & Tang, 2013; Thumthae, 2015) have also employed BEM theory in their works to optimize and evaluate the various types of wind turbine or wind energy systems. Karimian and Rasekh investigated the performance of a floating offshore wind turbine using a mixed CFD-BEM framework (Shin, Lee, & Chang, 2019). They evaluated the aero-acoustic performance of a vertical axis wind turbine in separate research (Eggleston & Stoddard, 1987).

As mentioned earlier, the INVELOX wind turbine is one of the most efficient systems in the field of wind energy facilities. It has a significant impact on the annual energy production by the wind. The effect of the existence of turbine blades embedded in the venturi section of the INVELOX system has not yet been explored in the literature. Similarly, the study of the flow characteristics in a rotor cascade and developing a simple analytical model to predict the power extracted by this turbine series are still new and attractive research activities. These topics will be covered in the course of this research. Furthermore, this research presents the development of an optimal wind turbine layout specifically designed for installation in the venturi section. The layout includes a unique distribution of blade chord and twist angles, which have been optimized for maximum performance and efficiency. In the present study, BEM theory, with an acceptable capability for design and analysis of wind turbines, is assumed. Prandtl's tip and hub loss factors, as well as turbulent wake corrections, have been taken into account in deriving the optimum chord and pitch angle distribution for the proposed wind turbine geometry. The wind turbine geometry will then be analyzed from an aerodynamic perspective, considering these factors to ensure optimal performance.

2. Basic equations and flow modeling

BEM theory is a combination of blade element theory and momentum theory. In this theory, it is first assumed that each blade can be divided into a limited number of independent elements. Each of these elements produces a circular flow. Upon applying this division, the momentum theory is used to determine induction velocities in the axial and tangential directions in each of those blade sections. Then, the aerodynamic forces for each section are calculated using the blade element theory. Finally, by considering the input conditions of the problem and repeating the analysis, the total aerodynamic forces acting on the wind turbine can be extracted for each set of conditions.

2.1. Momentum theory

In momentum theory, a control volume around the rotor is first assumed, as shown in Figure 2. The presence of the rotor plane in the control volume leads to a discontinuity in the pressure within the control volume. Finally, power and thrust can be calculated using the conservation of mass equations. In order to increase the accuracy of the momentum theory, the effect of wake rotation is considered. However, the upstream airflow of the rotor is still non-rotating. It should be noted that in the case of a horizontal wind turbine, the rotation of the wake is opposite to the rotation of the blades on the rotor. In the flow, the conservation of angular momentum can be applied. The wake rotation, as well as the rotation of the operator disk, results in a tangential component of velocity.
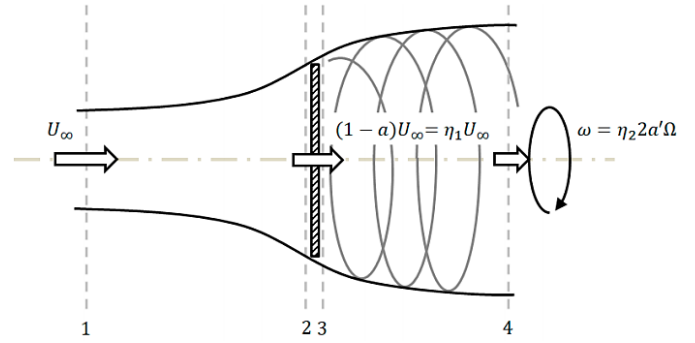
Figure 2. A control volume around a rotor with wake rotation (Shin, Lee, & Chang, 2019)

The angular velocity of the rotor (ω) is higher than that of the wind flow (Ω), allowing us to assume, with acceptable accuracy, that the pressure of the free flow is equal to the far wake pressure. After the flow passes through the rotor and the effects of the rotor rotation are applied, the value of the angular velocity of the flow increases and reaches $\Omega + \omega$. However, the axial and tangential components of the velocity will remain constant. Finally, based on Bernoulli's law, the thrust force can be derived as follows:

$$dT = 4\pi\rho a(1-a)U_\infty^2 r dr \tag{1}$$

where a is the axial induction factor. Based on the angular momentum conservation law, the rotor torque can be obtained as follows.

$$dQ = 4\pi\rho U_\infty a'(1-a)\Omega r^3 dr \tag{2}$$

where a' is the tangential induction factor and is defined as $a' = \frac{\omega}{2\Omega}$. We know that the power produced by each radial element of the blade is related to the torque, which is expressed as $dP = \Omega dQ$. Thus, using Equation 2, we have:

$$dP = \frac{4}{\lambda^2}\rho A U_\infty^3 d(1-a)\lambda_r^3 d\lambda_r \tag{3}$$

Therefore, the power coefficient can be obtained as follows:

$$C_P = \frac{8}{\lambda^2}\int_{\lambda_h}^{\lambda} a'(1-a)\lambda_r^3 d\lambda_r \tag{4}$$

2.2. Blade element theory

In order to develop the BEM theory for applying the conditions of the presence of the turbine in the venturi section of the INVELOX system, it is necessary to determine the geometric characteristics of the turbine blades used. The key to achieving this connection is blade element theory. In this method, a finite number of elements on the blade and along the blade span are considered, and the effective parameters, including force and momentum, are calculated for each of these elements. Finally, by integrating along the blade span, the total force and momentum on each blade can be obtained. Figure 3 shows an overview of how the blade is divided into a finite number of elements.
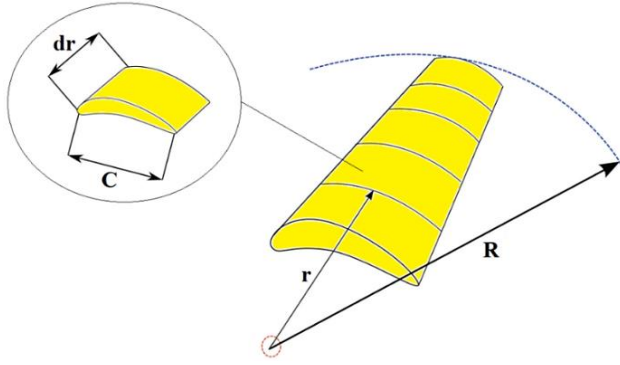
Figure 3. An overview of how a blade is divided into a finite number of elements

Figure 4 shows the details of the aerodynamic forces acting on the cross-section of a horizontal wind turbine blade. In this figure, α is the angle of attack, θ the pitch angle, ϕ the flow angle, F_n the tangential force or thrust, and F_t the normal force. The lift and drag forces are also perpendicular and tangent to the direction of relative velocity, respectively.
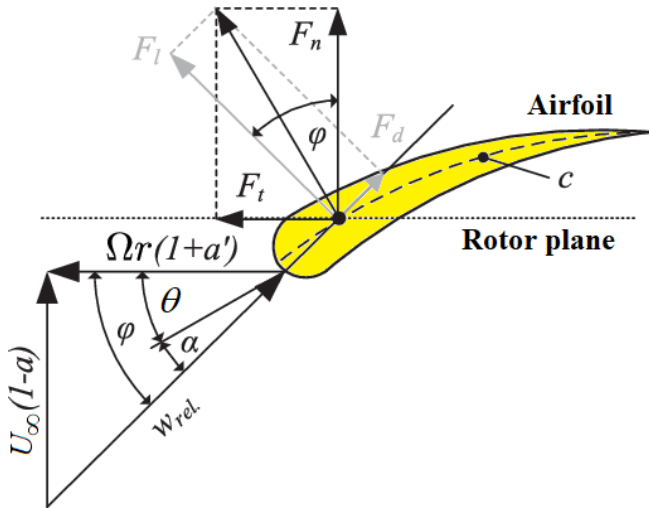
Figure 4. Details of the aerodynamic forces acting on the cross-section of a horizontal wind turbine blade

Assuming a certain number of elements on each blade, the thrust and torque on each element are calculated as follows:

$$dQ = \sigma \pi \rho \frac{(1-a)^2 U_\infty^2}{\sin^2 \phi} (C_L(\sin \phi) - C_d(\cos \phi)) r dr \qquad (5)$$

$$dT = \sigma \pi \rho \frac{(1-a)^2 U_\infty^2}{\sin^2 \phi} (C_L(\cos \phi) + C_d(\sin \phi)) r dr \qquad (6)$$

2.3. Blade element theory corrections

To increase the accuracy of problem-solving, Prandtl's loss factor and turbulent wake correction are applied to the blade element theory. The wing vortices for a rotor with a limited number of blades are quite different from a rotor with an infinite number of blades. So far, the relationships are such that the number of blades is assumed to be infinite. Considering the limited number of blades and the application of the presence of vortices at the tip of each blade to the problem, force and momentum equations must be adjusted. Prandtl's loss factor

takes into account the effect of the disc discontinuity. Prandtl's loss factor, which includes tip and hub loss factors, is defined as follows:

$$F = \left[\frac{2}{\pi} \cos^{-1} \left(e^{-\frac{B}{2} \frac{R-r}{r\sin(\phi)}} \right) \right] \left[\frac{2}{\pi} \cos^{-1} \left(e^{-\frac{B}{2} \frac{r-R_{hub}}{r\sin(\phi)}} \right) \right] \qquad (7)$$

When the axial induction factor exceeds 0.5, the velocity at the outlet of the control volume becomes negative. This indicates that the momentum theory becomes invalid for axial induction factors greater than 0.5, and it cannot accurately predict the thrust coefficient of the wind turbine. Therefore, it is necessary to correct and modify the obtained relations. For this purpose, several relations were utilized by Glauert (Glauert, 1926), Eggleston (Eggleston & Stoddard, 1987), Buhl (Buhl Jr, 2005), and Burton (Burton et al., 2011), the most important of which are given in Table 1.

Table 1. Different models presented for the turbulent correction

Corrected thrust coefficient	Critical axial induction factor	Model
$4a(1 - \frac{(5-3a)a}{4})F$	0.2	Glauert (Glauert, 1926)
$1.816 - 4(\sqrt{1.816} - 1)(1-a)$	0.3262	Burton (Burton et al., 2011)

2.4. BEM theory

Once the momentum and blade element theories have been fully explained, they can now be combined to derive the required relationships. In this way, the obtained thrust forces for each radial element along the blade span are equated by the momentum theory and the blade element theory. As a result, the axial induction factor and the tangential induction factor are obtained using the two following relations.

$$a = 1 / \left(\frac{4F\sin^2(\phi)}{\sigma C_n} + 1 \right) \qquad (8)$$

$$a' = 1 / \left(\frac{4F\sin(\phi)\cos(\phi)}{\sigma C_t} - 1 \right) \qquad (9)$$

Equation 8 holds only if the value of the axial induction factor is less than the critical value ($a < a_c$). If the axial induction factor is greater than the critical value ($a > a_c$), the value of the thrust coefficient must then be used using one of the various models proposed to correct the turbulent wake (as shown in Table 1). Accordingly, by applying the thrust equalization obtained for each radial element along the blade span using the momentum theory and the blade element theory, the new value of the axial induction factor can be determined. These modified values for the axial induction factor for the models presented in Table 1 are given in Table 2.

Table 2. Corrected axial induction factor for various models proposed for the turbulent wake correction

Corrected axial induction factor	Critical axial induction factor	Model
$\left(0.143+\sqrt{0.0203-0.6427\left(0.889-C_T\right)}\right)/F$	0.2	Glauert (Glauert, 1926)
$1+\dfrac{C_T-1.816}{4\left(\sqrt{1.816}-1\right)}$	0.3262	Burton (Burton et al., 2011)

By specifying the modified axial induction factor, the values of the axial induction factor for each element along the blade span can be calculated using an iterative pattern. After ensuring the axial and tangential induction factors, it is now possible to calculate the thrust, momentum, and power using the following equations.

$$T = B\sum_{i=1}^{N} F_{n_i} \tag{10}$$

$$Q = B\sum_{i=1}^{N} F_{t_i} r_i \tag{11}$$

$$P = \Omega B\sum_{i=1}^{N} F_{t_i} r_i = \Omega Q \tag{12}$$

3. Benchmark system geometry

3.1. Baseline Invelox characteristics

Figure 5 shows the three-dimensional geometry of the studied INVELOX wind turbine system. In this figure, the dimensions of this system are also depicted. The dimensions of the geometry are given in Table 3.
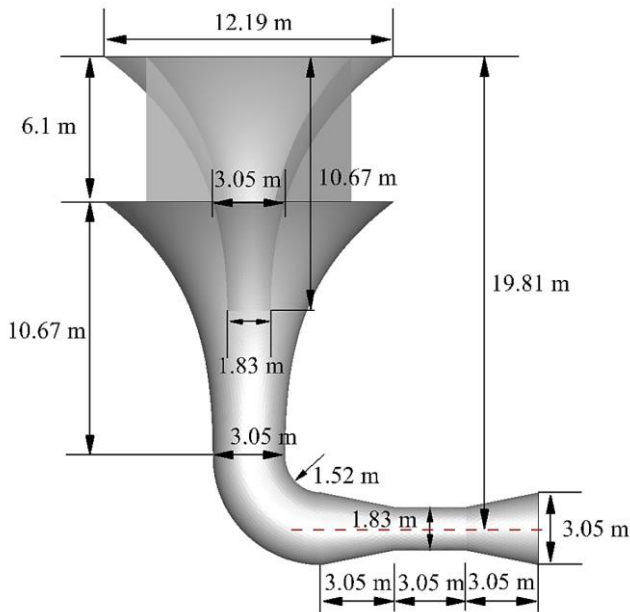
Figure 5. Dimensions of the studied INVELOX wind turbine system (Ding & Guo, 2020)

Table 3. Geometric specifications of the INVELOX wind turbine system

Dimension (m)	Symbol	Parameter
12.192	$D_{Funnel,Upper}$	Upper funnel diameter
21.336	H	Overall height
10.668	H_{Funnel}	Funnel height
1.83	$D_{Funnel,Lower}$	Lower funnel diameter
6.096	H_{Inlet}	Inlet height
1.83	$D_{Venturi}$	Venturi diameter
3.048	D_{Outlet}	Outlet diameter

As shown in Figure 5, the INVELOX wind turbine system is designed to absorb wind flow from all directions in a 360-degree range and it, therefore, does not require adjusting directly or indirectly the direction of the turbine blades in the direction of the wind. In addition, there are four guide vanes at the inlet of the INVELOX wind turbine system, whose function is to control and direct the incoming wind current to the system. The wind flow absorbed by the inlet of the INVELOX wind turbine system is transmitted downwards and after passing through an elbow, it is radiated in the venturi section to the turbine blades installed on the ground and inside the horizontal channel of the INVELOX wind turbine system.

3.2. Blade geometry and optimum design

Given that the diameter of the venturi section of the INVELOX system provided by Allaei and Andreopoulos (Allaei & Andreopoulos, 2014; Allaei, Tarnowski, & Andreopoulos, 2015) is 1.83 m, and according to data presented in reference (SnehalNarendrabhai & Desmukh, 2018), the diameter of the optimized turbine is considered to be 1.73 m. It should be noted that the initial 0.05 m radius of the blades is considered for the hub. That is, indeed, the length of each blade is equal to 0.82 meters. In a report presented by Tangier and Somers (Tangler & Somers, 1995), for blades with a length of 1 to 5 meters, NREL-S823 and NREL-S822 airfoils are recommended for the sections near the root and the sections near the tip of the blade, respectively. Due to the short length of the blades and the limited diameter of the venturi section of the INVELOX system, this paper uses NREL-S823 airfoil for all blade sections. According to the data of reference (Anbarsooz, Hesam, & Moetakef-Imani, 2017) and by considering the velocity of wind flow at the venturi section of the INVELOX system, the local Reynolds number at the venturi will be $Re = \dfrac{\rho VD}{\mu} = \dfrac{1.2\times11\times1.828}{1.8\times10^{-5}} = 1.341\times10^{6}$. The data associated with the NREL-S823 airfoil at Reynolds number 10e6 is shown in Table 4.

Table 4. Data on the NREL-S823 airfoil at Reynolds number 1000000

Paremetr	Value
Airfoil type	NREL-S823
N_ critical	9
$\left(C_L/C_D\right)_{max}$	101.5
α_{opt}	6.25°
$C_{L,\alpha_{opt}}$	1.0326
$C_{D,\alpha_{opt}}$	0.1017

Figure 6 shows the diagrams of the lift and drag coefficient of the NREL-S823 airfoil in the range of -180 to 180 degrees. Also, the information about the designed turbine is summarized in Table 5. By considering the optimum angle of attack for the NREL-S823 airfoil at the design point as well as the elements with a length of 0.01 on the blade, the optimum chord distribution and optimum pitch angle distribution diagrams are obtained, as shown in Figure 7.
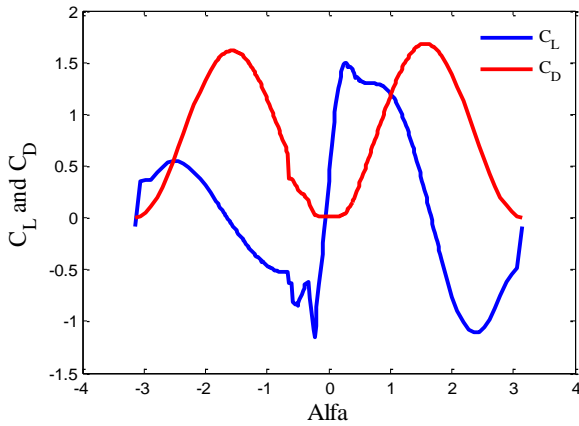

Figure 6. Lift and drag coefficient of the NREL-S823 airfoil
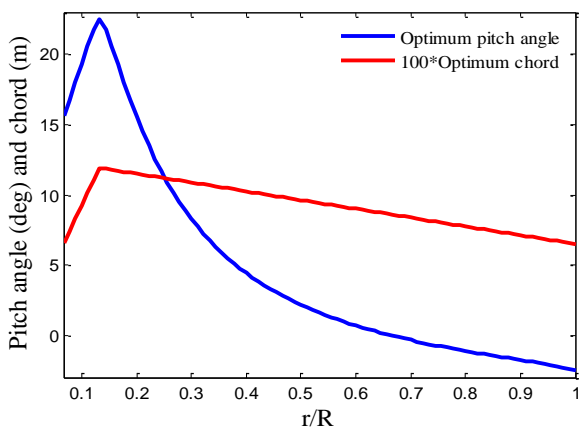
Figure 7. Optimum chord and optimum pitch angle distribution along the blade span

Table 5. Information of the designed turbine

Value	Characteristic
3	Number of blades
0.82 m	Length of each blade
1.73 m	Rotor diameter
0.0952 m	Hub diameter
From hub to 0.05 m	Circular airfoil
From 0.05 m to 0.8668 m	NREL-S823
	Airfoil type

4. Results and discussion

The results of the proposed BEM code in MATLAB can be illustrated in terms of two distinct groups. These two categories include the changes in different aerodynamic parameters versus the blade tip speed ratio and the spatial distribution of the forces along the blade length. This paper initially investigates the changes of different parameters in terms of the blade tip speed ratio. Subsequently, an analysis is conducted on the changes of

these parameters along the blade span. The paper begins with the validation and verification of the BEM code. Then, the results of two distinct parameter studies are discussed. Following that, the performance of the system is examined when multiple rotors are installed tandemly. A comparison of power and forces curves in terms of speed ratio and along the blade length is presented, leading to new practical insights.

4.1. Validation

The purpose of this section is to evaluate the validity of the developed code of the BEM theory. For this reason, the reference turbine and the blade geometry of Hsiao et al. (Hsiao, Bai, & Chong, 2013) are incorporated into the MATLAB code. In the mentioned study, the performance had been determined using 3 different approaches: experimental, numerical, and analytical. Results are compared with the experimental, numerical, and analytical results of the mentioned research. Hsiao et al. (Hsiao, Bai, & Chong, 2013) studied three different types of horizontal axis wind turbines with a diameter of 0.72 m. These three models include optimum blade shape (twisted and tapered), an un-tapered but twisted blade, and an un-tapered and un-twisted blade. Figure 8 illustrates the comparison of power coefficient results in terms of blade tip speed ratio obtained from the BEM code developed in this study. The comparison includes experimental data, numerical computations in Fluent software, and the results of the BEM method adopted by Hsiao et al. [18], which is incorporated for the optimum blade shape designed in their study. According to Figure 8, there is good agreement between the results obtained from the BEM code in the present work and the experimental, numerical, and analytical outputs of the reference. The geometry and performance of the optimum blade of (Hsiao, Bai, & Chong, 2013) are given in Table 6.
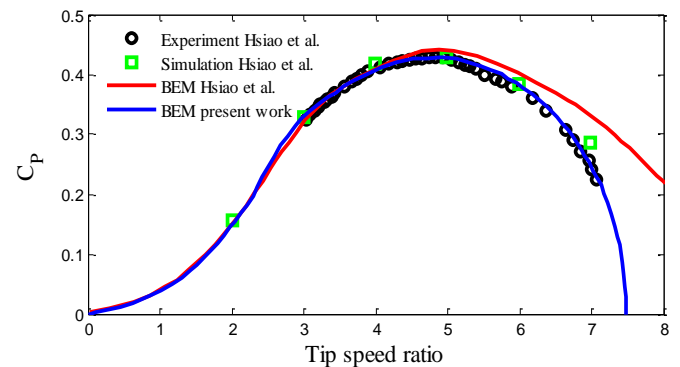

Figure 8. Comparison of the power coefficient results in terms of blade tip speed ratio between the results of Hsiao et al. (Hsiao, Bai, & Chong, 2013) and the present work

Table 6. Information of the optimum blade shape of Hsiao et al. (Hsiao, Bai, & Chong, 2013)

| Value	Characteristic
50	Rated power (Watt)
10	Rated wind speed (m/s)
5	Design tip speed ratio
3	Number of blades
5.5	Design angle of attack (deg)
NACA4418	Airfoil type

The minimum number of blade elements required for accurate code development is another important factor to consider. In this study, various choices of blade strip numbers were examined, ranging from 10 to 100 equally spaced nodes

along each blade. By comparing the accuracy and computation cost, the proper number of elements can be determined. The results show that a 20-element scheme is satisfactory with a confidence level of 95 percent in the performance indices. It should be noted that the validation study included the incorporation of Glauert wake correction as well as the Prandtl tip and hub loss factors.

4.2. Parametric study

4.2.1. Turbulent wake corrections

To analyze the various parameters considered in terms of the blade tip speed ratio, 20 elements on each blade are assumed, as mentioned in the previous section. Figure 9 compares the power coefficient variations in terms of blade tip speed ratio for two modes, the Glauert and the Burton turbulent wake correction. Both curves take into account the Prandtl's tip loss factor for a wind speed of 11 m/s and the number of blades of 3. In this diagram, only Prandtl's tip loss factor is included. The effect of Prandtl's hub loss factor was not traced. As can be seen, the two diagrams coincide until at the blade tip speed ratio of 5. At larger speed ratios, the difference grows up to about 7.9. The gradient is gradually increased until it reaches its maximum value, which typically occurs near the maximum power coefficient. After reaching the maximum value, the gradient remains constant. It is worth noting that the Burton turbulent wake correction curve is always below the Glauert turbulent wake correction curve. In Glauert's correction mode, the maximum power coefficient is 0.45 at a blade tip speed ratio of 7.91, while in Burton's correction mode, the maximum power coefficient is 0.39 at a blade tip speed ratio of 7.18.
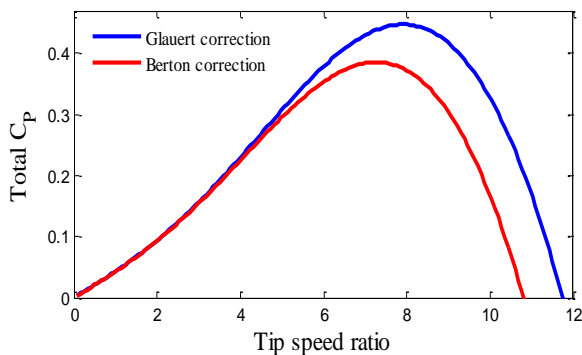
Figure 9. Comparison of power coefficient variations in terms of blade tip speed ratio for the two corrections of Glauert and Burton, taking into account Prandtl's tip loss factor for a wind speed 11 m/s and the number of blades (3)
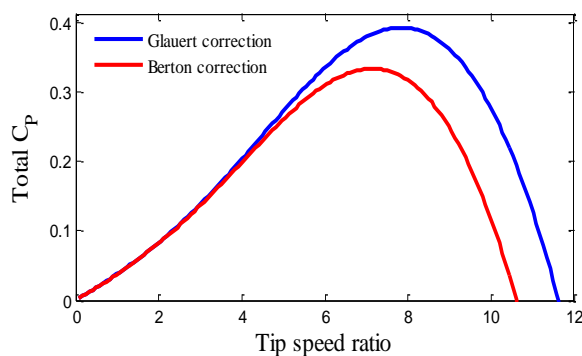
Figure 10. Comparison of power coefficient variations in terms of blade tip speed ratio for the two corrections of Glauert and Burton, taking into account the correction factor of Prandtl's tip and hub loss factor for both modes for wind speed of 11 m/s and the number of blades (3)

Figure 10 illustrates the comparison of power coefficient variations in terms of blade tip speed ratio for the Glauert and Burton turbulent wake correction modes, taking into account the Prandtl's tip and hub loss factor. With a wind speed of 11 m/s and 3 blades, including the Prandtl's hub loss factor results in a reduction of approximately 12% in the maximum power coefficient. This reduction is attributed to the limited flow contribution in the hub area. In the Glauert correction mode, the maximum power coefficient is 0.39 at a blade tip speed ratio of 7.83, while in the Burton correction mode, the maximum power coefficient is 0.33 at a blade tip speed ratio of 7.18. In other words, when accounting for the effect of Prandtl's tip and hub loss factor, the ratio of the maximum power coefficient is 0.88 for the Glauert correction and 0.87 for the Burton correction. However, the blade tip speed ratio at which the maximum power is achieved remains unchanged. It can be concluded that Prandtl's hub loss factor only reduces the power coefficient. Table 7 provides a comparison of the power coefficients for Glauert and Burton corrections with the inclusion of Prandtl's loss factor.

Table 7. Comparisons of the power coefficient for Glauert and Burton corrections and Prandtl's loss factor
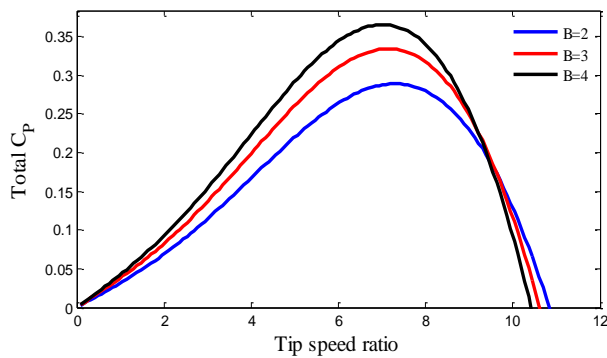
Tip speed ratio at maximum power coefficient	Maximum power coefficient	Model
7.9136	0.45	Glauert's correction and tip loss factor
7.83	0.39	Glauert's correction and tip and hub loss factor
7.18	0.39	Burton's correction and tip loss factor
7.18	0.33	Burton's correction and tip and hub loss factor

4.2.2. Blade numbers

Figure 11 presents a comparison of the power coefficient in relation to the blade tip speed ratio for different numbers of blades, taking into account the Glauert correction and Prandtl's tip and hub loss factor with a wind speed of 11 m/s. As can be seen, the number of blades installed on the hub has a significant impact on the amount of maximum power coefficient. For two blades, the maximum power coefficient is 0.329 and occurs at a blade tip speed ratio of 7.83. For three blades, the maximum power coefficient is 0.39 and happens at the mentioned ratio. Finally, for 4 blades, the maximum power coefficient is 0.442 and occurs at the mentioned ratio. Implications indicate that as the number of blades increases from 2 to 3, the maximum power factor is magnified by a factor of 1.19, and upon increasing the number of blades from 3 to 4, the maximum power factor is changed by a factor of 1.13. However, the tip speed ratio corresponding to these maximum power coefficients remains fixed and unchanged.
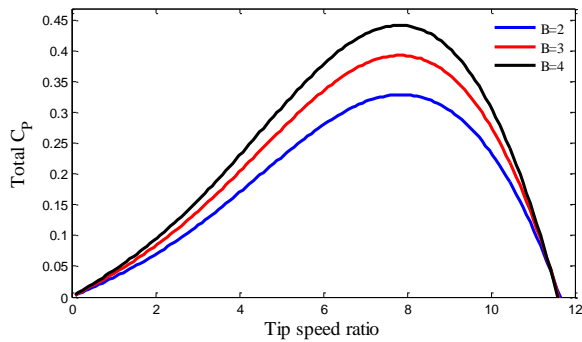
Figure 11. Comparison of the power coefficient in relation to the blade tip speed ratio for different blades, taking into account the correction of Glauert and Prandtl's tip and hub loss factor at a wind speed of 11 m/s

Figure 12. Comparison of the power coefficient in relation to the blade tip speed ratio for different numbers of blades, taking into account the correction of Burton and Prandtl's tip and hub loss factor at a wind speed of 11 m/s

Additionally, it is worth noting that the three curves intersect within the range of the blade tip speed ratio of 11.39 to 11.49. The specific intersection points are as follows: for the 3-blade and 4-blade configurations, the intersection occurs at a tip speed ratio of 11.39; for the 2-blade and 4-blade layouts, the intersection point is at a tip speed ratio of 11.45; and for the 2-blade and 3-blade configurations, the intersection is at a tip speed ratio of 11.49. It is interesting to observe that at low wind velocities and with little power being extracted, the sensitivity of the power to the number of blades becomes negligible.

Figure 12 depicts a similar comparison for Burton correction as well as the Prandtl's tip and hub loss factor. The wind speed is again 11 m/s. The maximum power coefficient and the corresponding tip speed are 0.29 and 7.34 for the 2-blade layout; 0.33 and 7.18 for the 3-blade layout; and 0.37 and 7.02 for the 4-blade rotor. By adding one more blade, the maximum power factor will be augmented by a factor of 1.16 while adding two blade will enhance the power factor by 1.27 factor. The tip speed ratio of these maximum power coefficients has changed very slightly. As mentioned before, regions of lower sensitivity are defined as the curve intersections (the tip speed ratio of 9.16 to 9.65). Table 8 illustrates the comparison of the power coefficient in the case of Glauert and Burton correction in terms of blade numbers.

Table 8. Comparisons of the power coefficient for various blade numbers for Glauert and Burton corrections
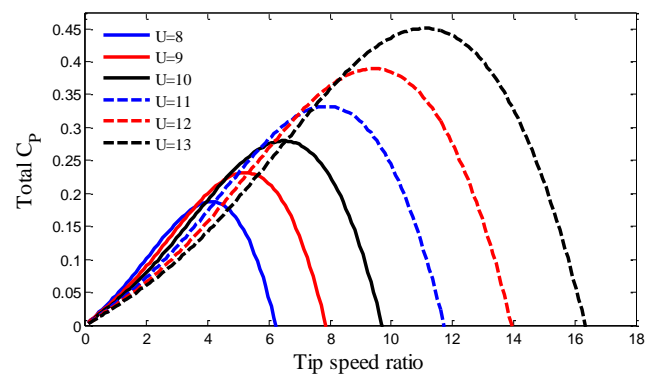
Tip speed ratio at maximum power coefficient	Maximum power coefficient	Blade numbers	Model
7.8319	0.3294	2	Glauert's correction and tip and hub loss factor
7.8319	0.39	3	
7.8319	0.4422	4	
7.34	0.29	2	Burton's correction and tip and hub loss factor
7.18	0.33	3	
7.02	0.37	4	

4.2.3. Wind velocity

Figures 13 and 14 illustrate the relationship between the power coefficient and the blade tip speed ratio for the 3-blade rotor, considering both the Glauert and Burton corrections. The wind speed contours ranging from 8 m/s to 13 m/s are also displayed. It is evident that as the wind velocity increases, the maximum power coefficient and the corresponding tip speed ratio also increase. The specific values of the maximum power coefficient and the corresponding tip speed ratio are provided in Tables 9 and 10. In Figure 15, the effect of the two mentioned corrections on the thrust coefficient is presented and compared in terms of the axial induction factor. The critical induction factor is specified in Table 1.
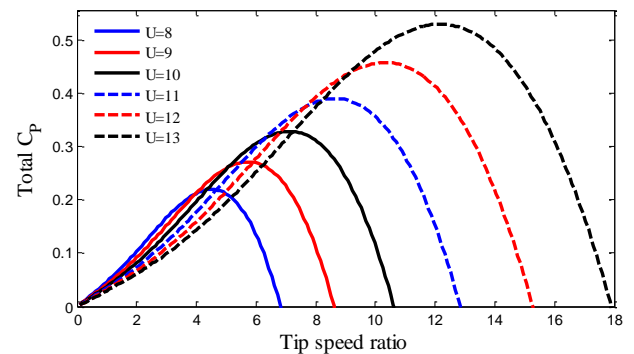
Figure 13. Comparison of the total power coefficient in terms of the blade tip speed ratio for different wind speeds, taking into account the Glauert correction and also Prandtl's both tip and hub loss factor for the number of blades (3)

Figure 14. Comparison of the total power coefficient in terms of the blade tip speed ratio for different wind speeds, taking into account the Burton correction and also Prandtl's both tip and hub loss factor for the number of blades (3)

Table 9. Comparisons of the power coefficient at different wind speeds for the Glauert correction and Prandtl's loss factor
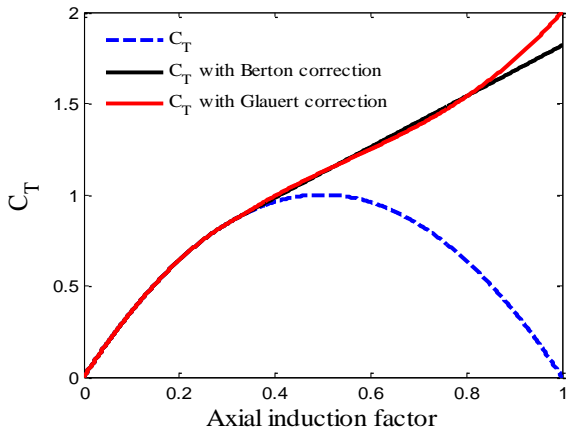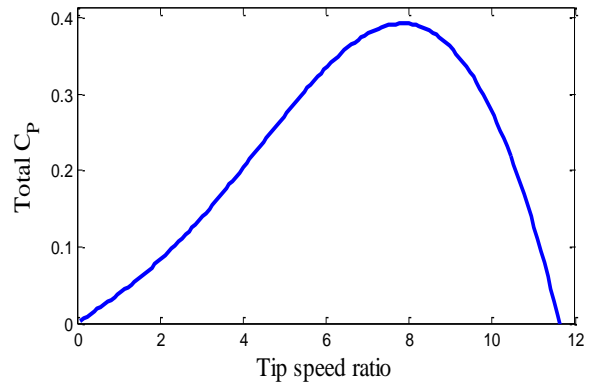
Tip speed ratio at maximum power coefficient	Maximum power coefficient	Wind speed
4.5323	0.2202	8
5.7107	0.272	9
7.161	0.3289	10
8.702	0.3909	11
10.3336	0.4582	12
12.1465	0.5306	13

Table 10. Comparisons of the power coefficient at different wind speeds for the Burton correction and Prandtl's loss factor

Tip speed ratio at maximum power coefficient	Maximum power coefficient	Wind speed
4.079	0.1874	8
5.2574	0.2314	9
6.5265	0.2797	10
7.8861	0.3323	11
9.4271	0.3893	12
11.0587	0.4506	13

4.2.4. Tip speed ratio

This section investigates the distribution of parameters along the blade length. It is necessary to determine the optimum design point (tip speed) according to the wind speed obtained in the venturi section of the INVELOX system, which is the blade tip speed ratio corresponding to the maximum power coefficient at a wind velocity of 11 m/s. According to Figure 16 depicting the power coefficient of a 3-blade rotor at a wind speed of 11 m/s, one may obtain the operating point as the power coefficient of 0.39 and blade tip speed of 7.83. All the corrections were considered. The rotational speed is expected to be 96 rpm. Table 11 provides other required data associated with the proposed turbine.

Figure 15. Thrust coefficient versus axial induction factor by Glauert and Burton corrections


Figure 16. Power coefficient diagram in terms of the blade tip speed ratio for the number of blades 3 and a wind speed of 11 m/s, taking into account the correction of Glauert and the effect of Prandtl's tip and hub loss factor

Table 11. Information of the designed wind turbine on the design point for the Glauert correction, Prandtl's tip and hub loss factor, wind speed of 11 m/s, and number of blades (3)

| Value	Characteristic
0.39	Power coefficient
7.83	Tip speed ratio
96	Rotational speed (rpm)

With the optimum operating point determined, it is now possible to plot the spatial distribution of performance indices. To increase the accuracy of diagrams and the resolution of data, 1000 elements on each blade are considered. The issue has been evaluated through the element number independency. Figure 17.a shows the power contribution of the span-wise elements in the nominal condition (velocity of 11 m/s and 96 rpm). As observed, there is an ascending trend in power from the blade hinge/anchor point (0.05 m) to the maximum chord length (0.12 m) and maximum pitch angle (22.58 degrees) occurrence. The pick value is 0.52 watts/m. After this point up to 0.9 m, power descends, similar to the chord length and pitch angle trend. By integrating the power curve of Figure 17.a, the total power generated by the entire rotor can be obtained using Equation 12. At a tip speed ratio of 7.82, the output power of a 3-blade turbine (installed in the venture part) is approximately 820 watts.
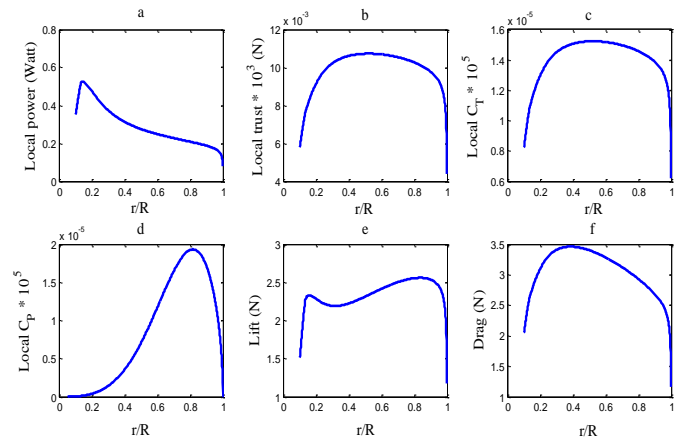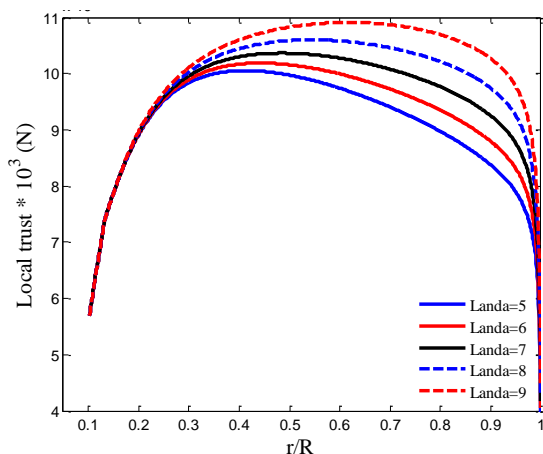

Figure 17. Local data diagram along the blade span at a wind speed of 11 m/s and rotational speed of 96 rpm

Figure 17.b shows the thrust force distribution along the blade at the same nominal point. The trend is initially ascending, while the slope gradually descends until the thrust reaches its maximum value at a radius of 0.46 m. At this point, thrust is 1.06e-2 N/m. after that the force is descending until it approaches 4e-3 N/m at the blade tip asymptotically. Through integration based on Equation 10, the applied axial force of a 3-blade rotor can be estimated as 22 N. The tip speed ratio is assumed to be 7.83.

Figure 17.c illustrates the lift force distribution in the same nominal operating condition. The force variation exhibits an ascending trend until reaching a local maximum at a radius of 0.14 m, where the force intensity is 2.3 N/m. Afterward, the lift slightly decreases until a local minimum at a radius of 0.28 m, with a load intensity of 2.2 N/m. This may be due to the reduction of both chord and twist in that location. The force will again reach the absolute maximum point located at a radius of 0.75 m and by a magnitude of 2.6 N/n. Figure 17.d shows the drag force diagram for the same conditions. The maximum value of 3.4 N/m at a radius of 0.35 m is experienced initially, followed by a deline toward the blade tip. It is notable that the general variation of the lift and drag force is affected by stall, which is probable especially adjacent to the hub. In other words, lift is expected to have a rising curve toward the tip, while drag is expected to have a falling curve toward the blade tip.
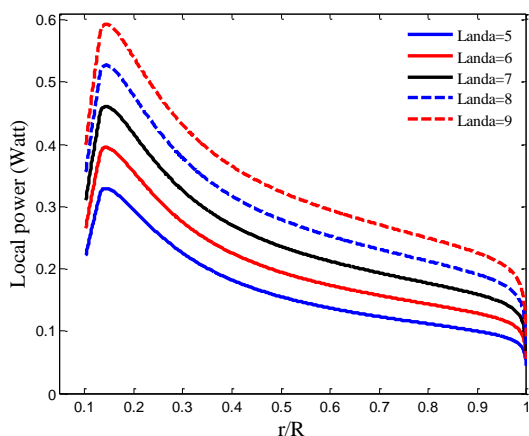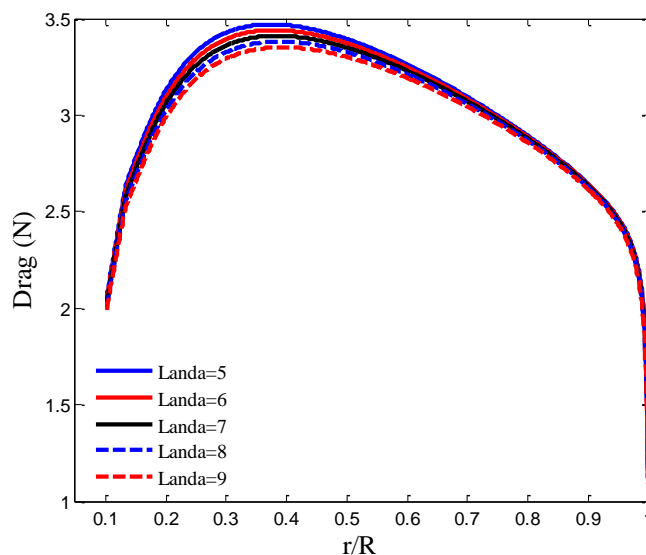

Figure 18. Local power diagram along blade span and for wind speed of 11 m/s and the number of blades (3) at a tip speed ratio of 5 to 9
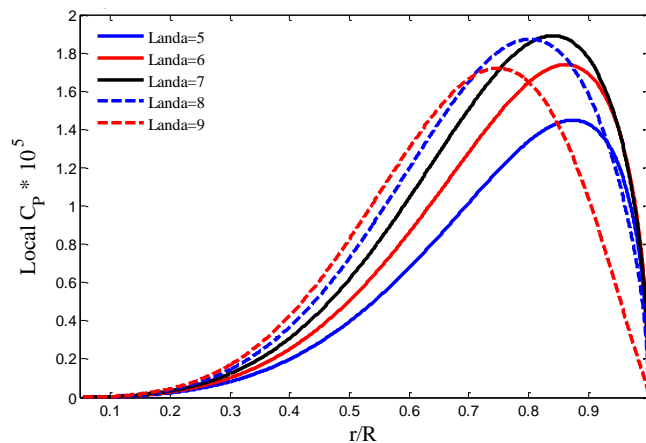

Figure 19. Local thrust diagrams along the blade span and at a wind speed of 11 m/s and the number of blades (3) at a tip speed ratio of 5 to 9
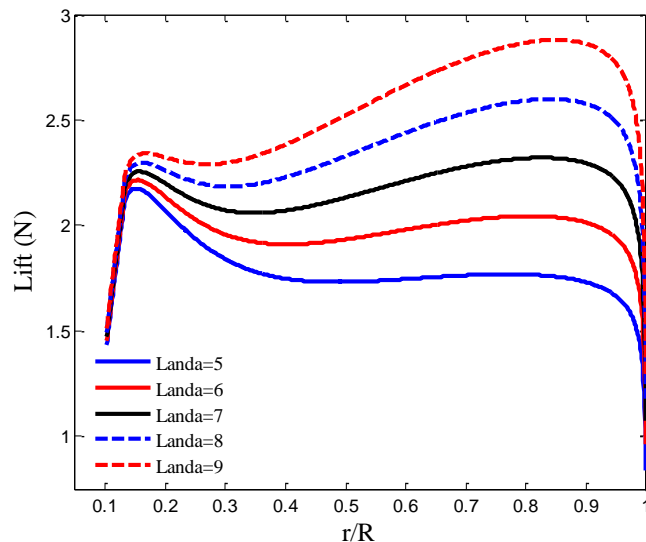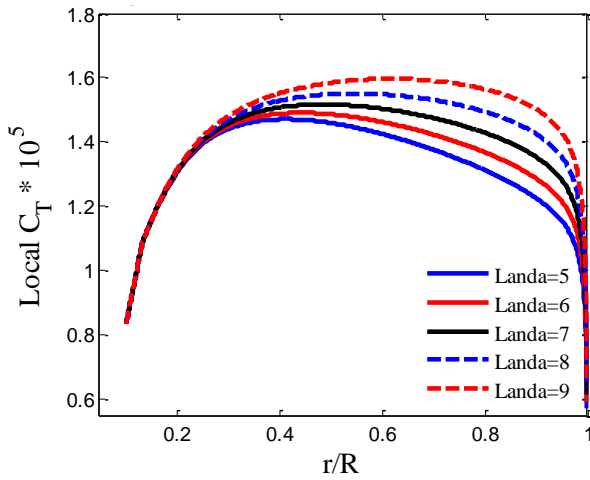

Figure 20. Local lift diagrams along blade span and for wind speed of 11 m/s and the number of blades 3 at a tip speed ratio of 5 to 9

Figure 21. Local drag diagrams along blade span and for wind speed of 11 m/s and the number of blades 3 at a tip speed ratio of 5 to 9

Figure 22. Local power coefficient diagrams along blade span and for wind speed of 11 m/s and the number of blades 3 at a tip speed ratio of 5 to 9

Figure 23. Local thrust coefficient diagrams along blade span and for wind speed of 11 m/s and the number of blades 3 at a tip speed ratio of 5 to 9

Figure 17.e shows the power coefficient distribution for the same nominal condition. As expected, the local C_P is affected by chord length and twist angle variation as well as the relative velocity magnitude and local angle of attack. Therefore, C_P may increase in value at a radius of 0.72 m and by a magnitude of 0.28 1/m. Figure 17.f depicts the thrust coefficient in the same operating condition. As may be seen, the general trend of C_T is quite similar to the thrust force diagram shown in Figure 17.b. Figures 18 to 23 depict the power, thrust, lift, drag, power coefficient, and thrust coefficient variation along the blade length. The wind velocity is 11 m/s and the number of blades is assumed 3. Different tip speed ratios (5 to 9) are presented. As can be seen, except for the power coefficient and drag force, other indices increase at the blade tip speed ratio.

Figure 21 shows that as the blade tip speed ratio increases, the drag force decreases. Considering Figures 22 and 16, one may realize that as the blade tip speed ratio increases, the maximum local power coefficient increases. The location moves away from the blade tip. However, at a tip speed ratio of 7, the trend changes. Follwoing further increase in the tip speed ratio, the maximum local power coefficient will decrease while its location still moves away from the blade tip. The same trend can be seen in Figure 16. The force variation exhibits an ascending trend until reaching a local maximum at a radius of 0.14 m, where the force intensity is 2.3 N/m. Afterward, the lift slightly decreases until a local minimum at a radius of 0.28 m, with a load intensity of 2.2 N/m.

4.3. Investigating the performance of multiple wind turbines

Assuming no wind turbine in the venturi section of the INVELOX wind system or supposing the free or no-load wind turbines may lead to minimum obstruction in the flow. It is implied that the velocity of the flow at the inlet of the venturi section will be approximately equal to the result of the numerical solution performed in Fluent software, which is 11 m/s. However, if the wind turbines installed in the system extract power and bear the load, then the flow is partially blocked (Ryi et al., 2015). The presence of this obstacle not only causes a pressure drop, but also affects the flow rate in the venturi section. Figure 24 shows a simple model to compute such attenuation due to the presence of wind turbines. As can be seen, if the effect of the operating wind turbine is considered

as a blockage, then flow velocity declines. Of course, if 2 or 3 turbines are mounted on the venturi section (as a cascade), the pressure drop or obstruction in the flow will be higher.
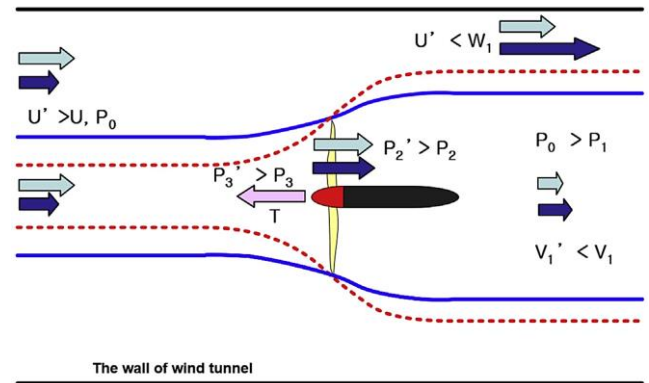
Figure 24. Effect of wind turbine on flow as a blockage

To simply estimate the velocity change, one can use the thrust force estimation by the BEM method. The thrust is:

$$T = \dot{m}\Delta U \tag{13}$$

Therefore, we have:

$$\Delta U = \frac{T}{\rho A U} \tag{14}$$

The total amount of thrust force via BEM code is equal to 28.01 N when the inlet velocity of 11 m/s is assumed. Through Equation 14, the velocity change is 0.83 m/s. Through this correction, the new estimate of 10.17 m/s can be computed. To calculate the correct flow velocity entering the first turbine, one may use a zero-order formula relating the performance of the INVELOX wind system to the output power extracted from the set of wind turbines installed in the venturi. By selecting an initial guess for the total extracted power, the flow velocity before the first stage of turbines can be estimated. Consequently, by using the BEM code, the extracted power will be calculated. The difference between the power obtained in this step and the assumed power (the guess value) simply determines the iterated error. By repeating the algorithm, the power and velocity will converge. In fact, the power extracted from the turbine cascade depends on the flow rate at the venturi inlet, while the velocity itself is a function of power. The algorithm is given in Figure 25. A simple formula concerning the venturi inlet velocity and the power extracted is:

$$U = \left(\frac{2P}{\rho A}\right)^{\frac{1}{3}} \tag{15}$$

Patel and Desmokh (SnehalNarendrabhai & Desmukh, 2018) investigated this issue via a numerical solution approach. Since the dimensions of the INVELOX wind turbine system used in the present work are consistent with those provided by Patel and Desmokh (SnehalNarendrabhai & Desmukh, 2018), to ensure the proposed approach, a new case study was adopted. The goal is the estimation of flow retardation due to operating turbines. The input velocity of 6.7 m/s and the same data presented by Patel and Desmokh (SnehalNarendrabhai &

Desmukh, 2018) (rotor radius 0.87 m; hub radius 0.05 m; and airfoil sections NREL-S801, NREL-S803, and NREL-S804) were implemented. The results are presented in Table 12. As can be seen in (SnehalNarendrabhai & Desmukh, 2018), the flow velocity in venturi was calculated at 12.38 m/s for no turbine case. The results of the iterative approach, validating the proposed approach, demonstrate the effect of wind turbine presence on the flow velocity in the venturi section. These results are presented in Table 13.

Table 12. Validation of the iterative approach of the effect of the turbine on the velocity in the venturi section

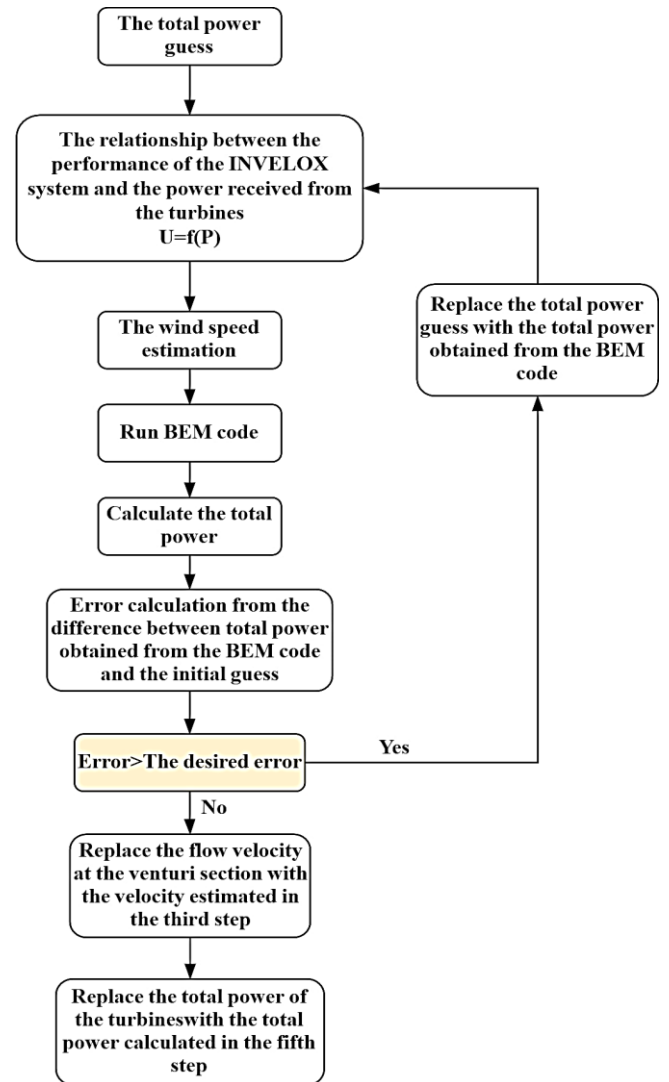|	Free flow velocity (m/s)	Flow velocity in venturi section (m/s) *	Speed ratio	Error (%)
Patel and Desmokh (SnehalNarendrabhai & Desmukh, 2018)	6.7	11.9906	1.7896	
The iterative approach applied to reference (SnehalNarendrabhai & Desmukh, 2018) data	6.7	11.7897	1.7597	1.68

* Considering the effect of the presence of a wind turbine

Table 13. Results of the iterative approach of the effect of wind turbine presence on the flow velocity in the venturi section

Free flow velocity (m/s)	Optimal rotational speed (rpm)	Regardless of the effect of the presence of wind turbines			Considering the effect of the presence of wind turbines		
		Flow velocity in venturi section (m/s)	Optimum tip speed ration	Extracted power (Watt)	Flow velocity in venturi section (m/s)	Optimum tip speed ration	Extracted power (Watt)
6.7	96	10.17	8.4989	665.16	9.86	8.7632	649.073

Table 14. Comparison of data obtained by the iterative approach with the referenced results (SnehalNarendrabhai & Desmukh, 2018)

	Free flow velocity (m/s)	Flow velocity in venturi section without turbine (m/s)	Flow velocity in venturi section with turbine (m/s)	Speed ratio
The iterative approach	6.7	10.17	9.86	1.0311
Patel and Desmokh (SnehalNarendrabhai & Desmukh, 2018)	6.7	12.38	11.9906	1.0321

**Figure 25.** Algorithm of the effect of wind turbines operating on the flow velocity in the venturi section

As can be seen, the flow velocity decreases from 10.17 m/s to 9.86 m/s due to the impact of the presence of the wind turbine. Table 14 makes a comparison between the above approach and the referenced results (SnehalNarendrabhai & Desmukh, 2018), thus approving the accuracy of the simple proposed approach. The flow velocity passing through the turbine is:

$$U_2 = \frac{U_1 + U_3}{2} \tag{16}$$

Assuming the flow velocity at the venturi inlet as 10.17 m/s and the flow velocity at the first rotor section as 9.86 m/s, the values of the desired velocities can be estimated (Table 15). The velocity profile in the venturi section is presented in Figure 26 for the arrangement of 3 wind turbines. It should be mentioned that the due to the repetitive nature of the presented algorithm and based on the extracted results in the full convergence state of the algorithm, the impact of wake of each turbine on the next turbine is incorporated implicitly in the presented iterative algorithm.

Table 15. Flow velocity values assuming the presence of three wind turbines

| Location	Flow velocity values (m/s)
Venturi Input (U1)	10.17
Before the first turbine (U2)	9.86
After passing the first turbine (U3)	9.5526
Before the second turbine (U2)	9.2644
After passing the second turbine (U3)	8.9762
Before the third turbine (U2)	8.7054
After passing the third turbine (U3)	8.4346
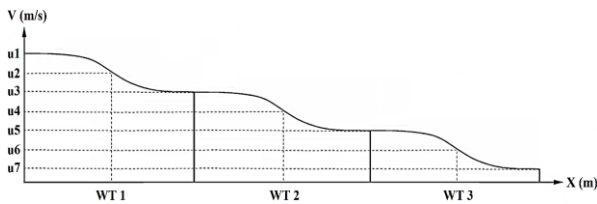
**Figure 26.** Speed diagram in the direction of the venturi section, assuming the presence of three wind turbines

Power, thrust force, thrust coefficient, power coefficient, lift, and drag diagrams along blade span are given in Figures 27 to 32 for the 3-wind-turbine layout. Except for the power coefficient and drag, the values of power, thrust, lift, and thrust coefficient decrease along the section. An interesting factor that can enhance the overall efficiency is to determine how much the second and third turbines should be used.
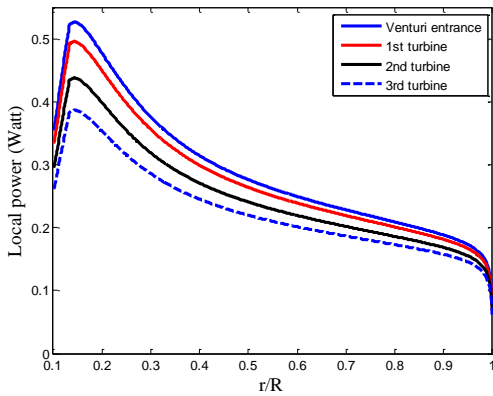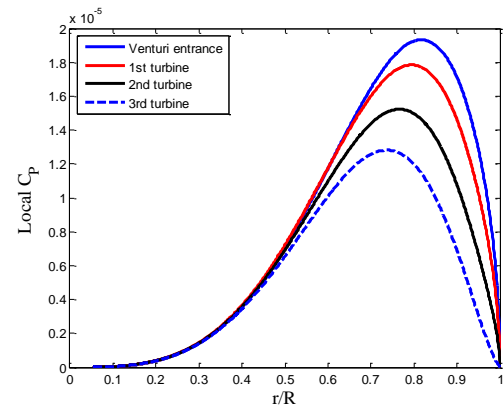
Figure 27. Power diagram along the blade span, assuming the presence of three wind turbines in the venturi section
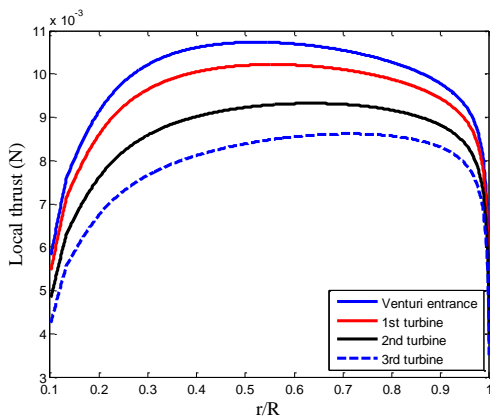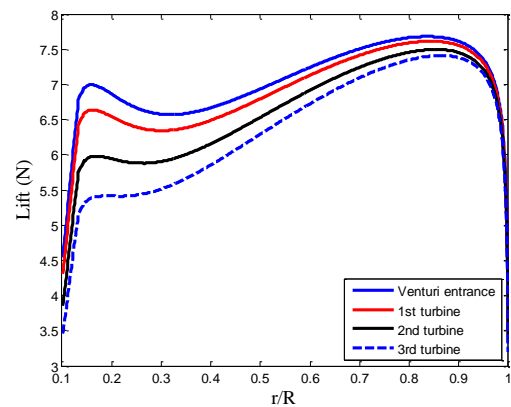
Figure 28. Thrust diagram along blade span, assuming the presence of three wind turbines in the venturi section
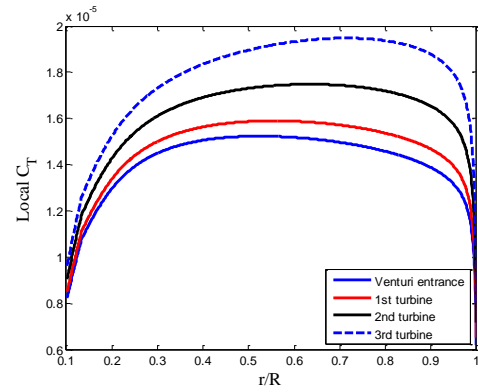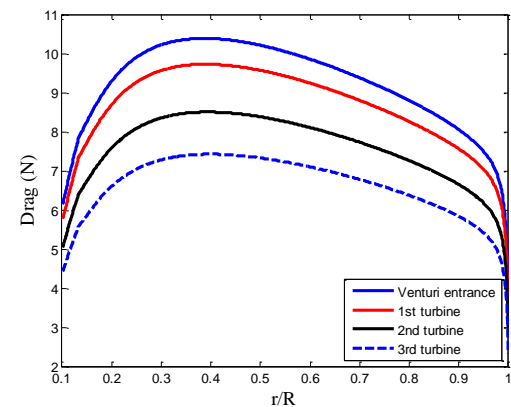
Figure 29. Thrust Coefficient diagram along blade span, assuming the presence of three wind turbines in the venturi section

Figure 30. Power coefficient diagram along blade span, assuming the presence of three wind turbines in the venturi section

Figure 31. Lift diagram along blade span, assuming the presence of three wind turbines in the venturi section

Figure 32. Drag diagram along blade span, assuming the presence of three wind turbines in the venturi section

Table 16 shows the power extracted from each turbine, and Table 17 shows the total power output for one, two, or three wind turbines located in the venturi section.
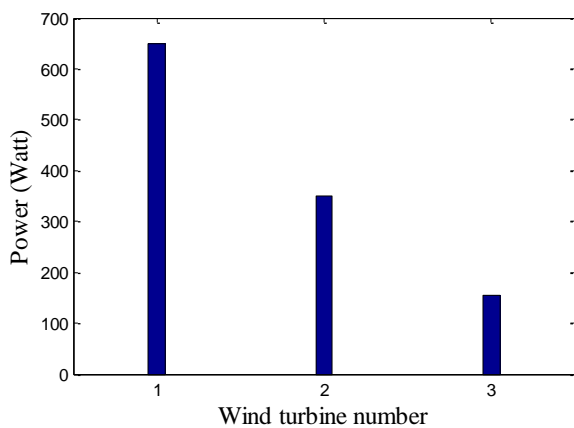
Table 16. Extracted power from each wind turbine

| Extracted power (Watt)	Wind turbine number
649.073	1
350.499	2
155.777	3

Table 17. Effect of number of turbines on extracted power

| Extracted power (Watt)	Wind turbines
649.073	1 turbine
999.572	2 turbines
1155.349	3 turbines

Figures 33 and 34 show the power graphs extracted from each turbine, as well as the effect of the number of turbines on the total power output. According to Table 17 and Figure 34, in the case of 2 and 3 turbines, the total power output is 1.54 and 1.78 times, respectively. The comparison of the output power ratios versus the number of turbines installed is shown in Figure 35, including the results of the present work and the experimental data from Allaei et al.

Figure 33. Extracted power from each wind turbine
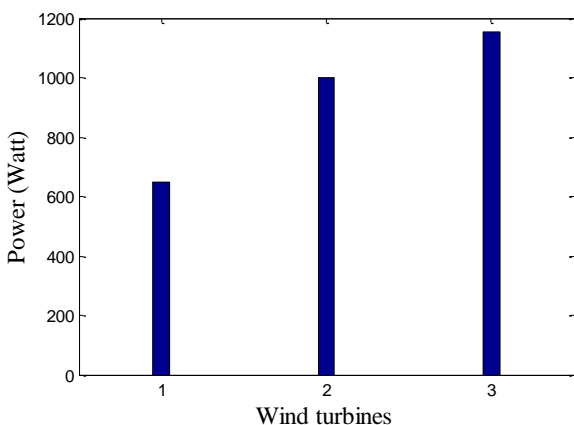
Figure 34. Effect of number of turbines on extracted power
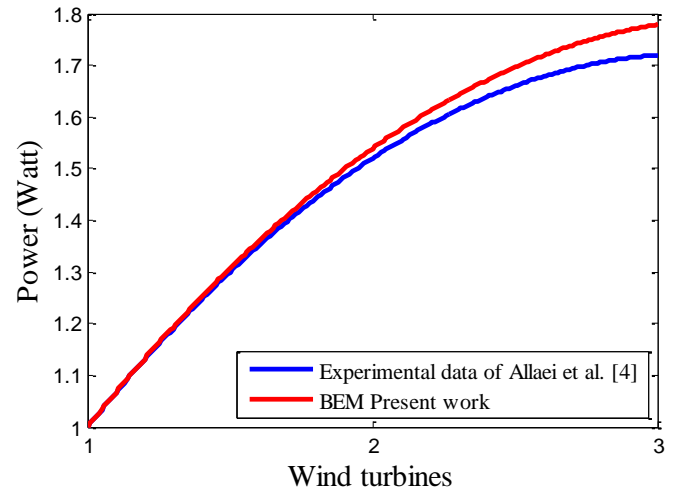
Figure 35. Comparison of output power ratios versus the number of turbines for experimental data from Allaei et al. (Allaei & Andreopoulos, 2013) and the present study.

5. Conclusions

In this paper, a semi-analytical code was developed to analyze the performance of the Invelox system. The output power ratios were compared between experimental data from Allaei et al. (Allaei & Andreopoulos, 2013) and the results obtained in the present work using BEM theory as the framework. The baseline Invelox system geometry was considered, and a suitable wind turbine was designed for the venturi section. The proposed model and code accounted for the Prandtl correction coefficient of the blade tip and hub, as well as the correction of the turbulent sequence. After validating the model, a parametric study was conducted, investigating changes in the tip speed ratio, chord length, and twist angle along the blade length. Performance quantities such as power, thrust, and lift force coefficients were calculated and analyzed for both individual sections and the complete rotor. The results of the study provide the following valuable insights:

- The comparison between Burton's correction and Glauert's correction shows that Burton's correction is more conservative, which is crucial for conceptual and basic design considerations. For instance, when considering 3 blades and a wind speed of 10.6 m/s, accounting for the Prandtl correction factor, the maximum power and the corresponding speed ratio were found to be 0.34 and 7.18, respectively, with Burton's correction. In contrast, with Glauert's correction, the maximum power and speed ratio were 0.39 and 7.83, respectively. The values of power, trust, and lifting force in the assumed Invelox system would increase with tip speed ratio, while the drag would decrease in the same conditions.

- Increase in the blade tip speed ratio led to increase in the maximum value of local power factor. This trend continued until the tip speed ratio of 7. Further increase in the blade tip speed ratio led to a decrease in maximum local power.

- The same pattern of variation was observed in the thrust coefficient and the torque coefficient in terms of

the blade tip speed. The issue can be addressed in the validation of semi-analytic codes.

- For the 2-turbine layout in the venturi section, the total power extracted was 1.54 times more than the single-turbine case, while for the 3-turbine case, the total power was 1.78 times.

Based on the findings of this study and the developed semi-analytical framework, it is possible to explore the optimization problems related to the geometry and arrangement of the cascade of wind turbines in the Invelox system. The authors are currently initiating research in this area to further enhance the system's performance and efficiency.

Acknowledgement

NOMENCLATURE

Symbol	Description
A	Area (m^2)
F	Prandtl's correction factor
a	Axial induction factor
a'	Rotational induction factor
C_L	Lift coefficient
C_D	Drag coefficient
$(C_L / C_D)_{max}$	Maximum lift to drag
C_P	Power coefficient
L	Lift force (N)
D	Drag force (N)
P	Power (Watt)
T	Tangential force (N)
Q	Torque (N.m)
U	Fluid velocity (m/s)
R	Rotor radius (m)
r	Local radius (m)
$C(r)$	Chord distribution (m)
λ	Tip speed ratio
R_{hub}	Hub radius (m)
Re	Reynolds number
B	Blade number
α	Attack angle (deg)
θ	Pitch or twist angle (deg)
θ_{opt}	Optimum pitch or twist angle (deg)
ϕ	Flow angle (deg)
ρ	Density (kg/m^3)
η	Efficiency
σ	Solidity
ω	Rotor rotational speed (rpm)

REFERENCES

1. Akour, S. N., & Bataineh, H. O. (2019). Design considerations of wind funnel concentrator for low wind speed regions. *AIMS Energy*, *7*(6), 728-742. https://doi.org/10.3934/energy.2019.6.728

2. Allaei, D., & Andreopoulos, Y. (2013). INVELOX: a new concept in wind energy harvesting. *Proceeding of ASME 2013 7th international Conference on energy Sustainability & 11th Fuel Cell Science, Engineering and Technology Conference ES-Fuel Cell*. https://www.semanticscholar.org/paper/INVELOX%3A-A-NEW-CONCEPT-IN-WIND-ENERGY-HARVESTING-Allaei-Andreopoulos/de606705b617e9fa7a3e5376362ecb46385a72d3

3. Allaei, D., & Andreopoulos, Y. (2014). INVELOX: Description of a new concept in wind power and its performance evaluation. *Energy*, *69*, 336-344. https://doi.org/10.1016/j.energy.2014.03.02

4. Allaei, D., Tarnowski, D., & Andreopoulos, Y. (2015). INVELOX with multiple wind turbine generator systems. *Energy*, *93*, 1030-1040. https://doi.org/10.1016/j.energy.2015.09.076.

5. Anbarsooz, M., Hesam, M. S., & Moetakef-Imani, B. (2017). Numerical study on the geometrical parameters affecting the aerodynamic performance of Invelox. *IET renewable power generation*, *11*(6), 791-798. https://doi.org/10.1049/iet-rpg.2016.0668.

6. Bavanish, B., & Thyagarajan, K. (2013). Optimization of power coefficient on a horizontal axis wind turbine using bem theory. *Renewable and sustainable energy reviews*, *26*, 169-182. https://doi.org/10.1016/j.rser.2013.05.009.

7. Billah, S. B., & Qasim, S. (2019). Development of MATLAB simulink model of Invelox to Analyze The Impact of Inlet Height On speed ratio. 2019 International Conference on Energy and Power Engineering (ICEPE), https://doi.org/10.1109/CEPE.2019.8726795.

8. Buhl Jr, M. L. (2005). *New empirical relationship between thrust coefficient and induction factor for the turbulent windmill state*. https://www.osti.gov/biblio/15016819

9. Burton, T., Jenkins, N., Sharpe, D., & Bossanyi, E. (2011). *Wind energy handbook*. John Wiley & Sons. https://books.google.com/books?hl=en&lr=&id=dip2LwCRCscC&oi=fnd&pg=PT16&dq=9.%09Burton,+T.,+Jenkins,+N.,+Sharpe,+D.,+%26+Bossanyi,+E.+(2011).+Wind+energy+handbook.+John+Wiley+%26+Sons.+&ots=IfxMSsMsz5&sig=WlZB85tL2kIVuPN5McjhX4d9gEU.

10. Ding, L., & Guo, T. (2020). Numerical study on the power efficiency and flow characteristics of a new type of wind energy collection device. *Applied Sciences*, *10*(21), 7438. https://doi.org/10.3390/app10217438.

11. Eggleston, D. M., & Stoddard, F. (1987). Wind turbine engineering design. https://www.osti.gov/biblio/5719832

12. Fereidoonnezhad, M., Tahani, M., & Esfahanian, V. (2017). Analysis of Ducted Wind Turbine using Surface Vorticity Method. 3rd International Conference of IEA, Iran, Tehran, https://www.sid.ir/FileServer/SE/559e20170301.pdf

13. Glauert, H. (1926). *The analysis of experimental results in the windmill brake and vortex ring states of an airscrew*. HM Stationery Office. https://books.google.com/books/about/The_Analysis_of_Experimental_Results_in.html?id=_JfFtgAACAAJ

14. Gohar, G. A., Manzoor, T., Ahmad, A., Hameed, Z., Saleem, F., Ahmad, I., Sattar, A., & Arshad, A. (2019). Design and comparative analysis of an INVELOX wind power generation system for multiple wind turbines through computational fluid dynamics. *Advances in Mechanical Engineering*, *11*(4), https://doi.org/10.1177/1687814019831475.

15. Golozar, A., Shirazi, F. A., Siahpour, S., Khakiani, F. N., & Gaemi Osguei, K. (2021). A novel aerodynamic controllable roof for improving performance of INVELOX wind delivery system. *Wind Engineering*, *45*(3), 477-490. https://doi.org/10.1177/0309524X20910986

16. Hosseini, S. R., & Ganji, D. D. (2020). A novel design of nozzle-diffuser to enhance performance of INVELOX wind turbine. *Energy*, *198*, 117082. https://doi.org/10.1016/j.energy.2020.117082

17. Hsiao, F.-B., Bai, C.-J., & Chong, W.-T. (2013). The performance test of three different horizontal axis wind turbine (HAWT) blade shapes using experimental and numerical methods. *Energies*, *6*(6), 2784-2803. https://doi.org/10.3390/en6062784.

18. Karimian Aliabadi, S., & Rasekh, S. (2019). Effect of Platform Surge Motion on the Performance of 5MW NREL Offshore Floating Wind Turbine. *Journal of Renewable Energy and Environment*, *6*(1), 8-14. https://doi.org/10.30501/jree.2019.95553.

19. Karimian Aliabadi, S., & Rezaey, S. (2022). Modeling of a wind energy harvesting INVELOX system by combination of numerical results and semi-analytical framework. *Sharif Journal of Mechanical Engineering*, *38*(2), 37-46. https://doi.org/10.24200/J40.2022.59289.1626.

20. Krishna, J. M., Bhargava, V., & Donepudi, J. (2018). BEM prediction of wind turbine operation and performance. *International Journal of Renewable Energy Research*, *8*(4). http://doi.org/10.4108/eai.27-10-2020.166771.

21. Kumar, N. M., Subathra, M., & Cota, O. D. (2015). Design and wind tunnel testing of funnel based wind energy harvesting system. *Procedia Technology*, *21*, 33-40. https://doi.org/10.1016/j.protcy.2015.10.006.

22. Lilley, G., & Rainbird, W. (1956). A preliminary report on the design and performance of ducted windmills. https://dspace.lib.cranfield.ac.uk/bitstream/handle/1826/7971/COA_Report_No_102_Apr_1956.pdf?sequence=1.

23. Liu, X., Wang, L., & Tang, X. (2013). Optimized linearization of chord and twist angle profiles for fixed-pitch fixed-speed wind turbine blades. *Renewable energy*, *57*, 111-119. https://doi.org/10.1016/j.renene.2013.01.036.

24. Masters, I., Chapman, J., Willis, M., & Orme, J. (2011). A robust blade element momentum theory model for tidal stream turbines including tip and hub loss corrections. *Journal of Marine Engineering & Technology*, *10*(1), 25-35. https://doi.org/10.1080/20464177.2011.11020241.

25. Nabil, T., Khairat Dawood, M., & Mansour, T. (2018). Design and Implementation of the Rotor Blades of Small Horizontal Axis Wind Turbine. *Journal of Renewable Energy and Environment*, *5*(2), 41-51. https://doi.org/10.30501/jree.2018.88633.

26. Nardecchia, F., Groppi, D., Lilliu, I., Astiaso Garcia, D., & De Santoli, L. (2020). Increasing energy production of a ducted wind turbine system. *Wind Engineering*, *44*(6), 560-576. https://doi.org/10.1177/0309524X19862760.

27. Rajan, A., & Ponta, F. L. (2019). A novel correlation model for horizontal axis wind turbines operating at high-interference flow regimes. *Energies*, *12*(6), 1148. https://doi.org/10.3390/en12061148.

28. Rezaey, S. (2020). Numerical investigation of a globe control valve and estimating its loss coefficient at different opening states. *European Journal of Computational Mechanics*, 549–576-549–576. https://doi.org/10.13052/ejcm1779-7179.294610.

29. Ryi, J., Rhee, W., Hwang, U. C., & Choi, J.-S. (2015). Blockage effect correction for a scaled wind turbine rotor by using wind tunnel test data. *Renewable energy*, *79*, 227-235. https://doi.org/10.1016/j.renene.2014.11.057.

30. Shin, J.-H., Lee, J.-H., & Chang, S.-M. (2019). A simplified numerical model for the prediction of wake interaction in multiple wind turbines. *Energies*, *12*(21), 4122. https://doi.org/10.3390/en12214122.

31. SnehalNarendrabhai, P., & Desmukh, T. (2018). Numerical simulation of flow through INVELOX wind turbine system. *Int J Renew Energy Resour*, *8*(1), 291-301. https://doi.org/10.20508/ijrer.v8i1.6753.g7303.

32. Solanki, A. L., Kayasth, B. D., & Bhatt, H. (2017). Design modification & analysis for venturi section of INVELOX system to maximize power using multiple wind turbine. *Int J Innovat Res Sci Technol*, *3*, 125-127. https://www.academia.edu/download/53485702/IJIRSTV3I11132.pdf

33. Supreeth, R., Arokkiaswamy, A., Hegde, K. M., Srinath, P., Prajwal, H., & Sudhanva, M. (2021). Analytical evaluation of performance of a small scale horizontal axis wind turbine rotor blade. AIP Conference Proceedings, https://doi.org/10.1063/5.0036766.

34. Tahani, M., Kavari, G., Masdari, M., & Mirhosseini, M. (2017). Aerodynamic design of horizontal axis wind turbine with innovative local linearization of chord and twist distributions. *Energy*, *131*, 78-91. https://doi.org/10.1016/j.energy.2017.05.033.

35. Tang, X., Huang, X., Peng, R., & Liu, X. (2015). A direct approach of design optimization for small horizontal axis wind turbine blades. *Procedia CIRP*, *36*, 12-16. https://doi.org/10.1016/j.procir.2015.01.047.

36. Tangler, J., & Somers, D. (1995). *NREL airfoil families for HAWTs: National Renewable Energy Laboratory*. https://www.osti.gov/biblio/10106095.

37. Thumthae, C. (2015). Optimum blade profiles for a variable-speed wind turbine in low wind area. *Energy Procedia*, *75*, 651-657. https://doi.org/10.1016/j.egypro.2015.07.478.

38. Vaz, J. R. P., Pinho, J. T., & Mesquita, A. L. A. (2011). An extension of BEM method applied to horizontal-axis wind turbine design. *Renewable energy*, *36*(6), 1734-1740. https://doi.org/10.1016/j.renene.2010.11.018.

39. Wibowo, T. T., Daulay, F. H., Suryopratomo, K., & Budiarto, R. (2018). Numerical study of the effect of geometry variation on the performance of innovative design wind speed enhancer. E3S Web of Conferences, https://doi.org/10.1051/e3sconf/20184201013.